Journal of Materials Chemistry C

Exploiting multiple percolation in two-terminal memristor to achieve a multitude of resistive states

Journal:	*Journal of Materials Chemistry C*
Manuscript ID	TC-ART-03-2021-000987.R2
Article Type:	Paper
Date Submitted by the Author:	15-Jun-2021
Complete List of Authors:	Foulger, Stephen; Clemson University, Materials Science & Bioengineering & COMSET Bandera, Iurii; Clemson University Grant, Benjamin; Clemson University Vilčáková, Jarmila; Univerzita Tomase Bati ve Zline, Polymer Centre; Saha, Petr; Univerzita Tomase Bati ve Zline, Polymer Science

SCHOLARONE™
Manuscripts

Exploiting multiple percolation in two-terminal memristor to achieve a multitude of resistive states

Stephen H. Foulger[a,b,*] Yuriy Bandera[a], and Benjamin Grant[a]

Center for Optical Materials Science and Engineering Technologies
[a]Department of Materials Science and Engineering
[b]Department of Bioengineering
Clemson University, Clemson, SC 29634-0971, USA

Jarmila Vilčáková[d,e], Petr Sáha[d,e]

[d]Polymer Centre, Faculty of Technology
[e]University Institute, Centre of Polymer Systems, Tomas Bata University in Zlín,
Tř. T. Bati 5678, 760 01 Zlín, CZE

*To whom correspondence should be addressed; e-mail: foulger@clemson.edu.

June 15, 2021

KEYWORDS: conjugated polymer, carbazole, low-power programming, dithieno[3,2-b:2,3-d]pyrrole (DTP)

Abstract

As the most likely prospect for the construction of neuromorphic networks, the emulation of synaptic responses with memristors has attracted attention in both the microelectronic industries and the academic environment. To that end, a newly synthesized hybrid conjugated polymer with pendant carbazole rings, that is, poly(4-(6-(9H-carbazol-9-yl)hexyl)-4H-dithieno[3,2-b:2',3'-d]pyrrole) (pC6DTP), was employed in the fabrication of a two-terminal memristor with a Al/pC6DTP/ITO configuration where the polymer was electrochemically doped. Signature biological synaptic responses to voltage spikes were demonstrated, such as potentiation & depression and spike timing dependent plasticity. The device was able to be programed through a 1 mV pulse, requiring only 100 fJ of energy. The voltage-dependent conductive nature of the polymer was speculated to occur through two synergistic mechanisms, one associated with the conjugation along the backbone of the conjugated polymer and one mechanism associated with the pendant heterocyclic rings.

1 Introduction

Although inorganic/organic memristors have been experiencing vigorous research activity since 2008 with the verified existence of Chua's 1971 proposed fourth basic element[1, 2], a number of researchers had observed the conductance switching properties of thin organic films as far back as the late 1960's and early 1970's[3–5]. Since then, organic bistable switching devices have been presented that were based on small molecules and polymers, as well as composite constructs, though the exact mechanism by which the transitions occur are under much debate and is speculated to be vastly disparate for differing organic materials and/or device constructs[6–12]. Nonetheless, the majority of memristive systems rely on some form of a stochastic creation/disruption of percolative paths inside a matrix to give rise to a binary (or abrupt) form of current switching. These systems were predominately developed to serve as a memory component in a von Neumann computer architecture[13] and, especially inorganic systems, have proven to be suitable for storing and processing information with numerous excellent attributes[2]. Conjugated polymers as two-terminal memory devices have been recently reviewed and the majority of the devices presented focused on developing materials appropriate

for dynamic random-access memory (DRAM), static random-access memory (SRAM), or write once read many (WORM) applications where a bistable conductivity switching response is appropriate[14].

The memory requirements for a von Neumann computer architecture differ greatly from biological inspired synaptic functions, where synaptic weights are modulated by the number and frequency of homogeneous spikes and take a continuity of values. There have been a number of review papers presented that discuss memristors which are focused on creating neuromorphic architectures[15–17]. Memristors in neuromorphic applications must exhibit reliable analog properties including non-abrupt switching transitions, continuously variable resistance states, and a predictable response. With these characteristics, a memristor may provide a simple and effective route for fabricating physical artificial neural networks which are independent of software programming[18].

Recently a non-volatile conjugated polymer-based electrochemical device was presented that exhibited characteristics of an artificial synapse and could be useful for neuromorphic computing[19]. The operation of the electrochemical device was based on the control of the conductivity of a conjugated polymer through the manipulation of its redox state. The main advantage of this design is that the barrier for state retention is decoupled from the barrier for changing states, though unfortunately this device is a three-terminal configuration and requires the simultaneous manipulation of the electrodes to achieve a write or read statement, adding complexity to the design and raising challenges to creating simple two-terminal printed devices, a point of interest with solution-processable materials.

Because of their potential for mass production through printing on flexible, as well as non-conformal, substrates, two-terminal organic/polymeric memristors for synaptic mimicry have been receiving significant research interest and their progress has been reviewed[17, 20]. As indicated earlier, most approaches to building two-terminal polymeric memristors focus on converting an insulating polymer or composite into a conductive material through a simple one dimensional percolation approach whereby a percolation threshold is transitioned. The result is an abrupt & binary switching from an insulator to conductor with limited repeatability. To achieve an analog response with a multitude of resistive states, one can imagine focusing not on the percolation threshold but in the region *post* percolation where a scaling relationships holds and the conductivity can be varied by orders of magnitude through smooth & continuous transitions with small variations in the percolation network[21]. We propose a methodology to achieve this aim through a multiple percolation approach which employs a hybrid conjugated polymer with pendant heterocyclic rings. These features give rise to two independent but synergistic paths to achieving the percolation network[22]. To this end, we focus on a class of conjugated polymer based on a dithieno[3,2-b:2,3-d]pyrrole (DTP) backbone.

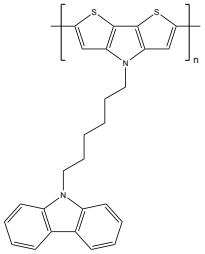

Figure 1: Poly(4-(6-(9H-carbazol-9-yl)hexyl)-4H-dithieno[3,2-b:2',3'-d]pyrrole) (pC6DTP).

Figure 1 presents the structure of the repeat unit of the conjugated polymer (poly(4-(6-(9H-carbazol-9-yl)hexyl)-4H-dithieno[3,2-b:2',3'-d]pyrrole) (hereafter called pC6DTP) employed in this effort. DTP-based polymers have found widespread applications in photovoltaic[23], electrochromic[24], energy storage[25], biosensing[26], thin-film transistor[27], OLED[28] and bistable memory[29] devices. An electron-rich heterocyclic compound with a fused-ring structure enhances the effective conjugation of DTP by increasing planarity in the polyDTP backbone and improved orbital overlap. In order to achieve continuous analog resistive states through a synergistic multiple percolation mechanism, the inherent conductivity of the DPT conjugated backbone is coupled with pendant groups in the form of electroactive carbazole moieties. The use of pendant carbazole moieties in creating memristors with a bistable switching response through field-induced conformational rearrangements of the pendant rings has been previously presented in the literature with both non-conjugated[10, 11, 30–32] and conjugated[33–36] polymers. In the current system, the DTP backbone is polymerized and oxidized to create the static percolating network that defines the system's baseline conductivity. Coupled to the backbone are flexible pendant carbazoyl moieties which can rearrange to give conductive pathways when the rings experience

electronic overlap. In essence, one percolating mechanism achieves electrical percolation of the system (e.g., DTP) while the second mechanism (e.g., carbazoles) increases or decreases the network redundancy of the system resulting in smooth resistivity changes.

2 Results and discussion

Monomers incorporating dithieno[3,2-b:2,3-d]pyrrole (DTP) can be chemically and electrochemically polymerized[24, 37–40]. **Figure 2a** presents the 1st and 50th cyclic voltammogram of the C6DTP monomer (cf. **Figure 1**) in an acetonitrile (ACN) / 0.1 M $TBAPF_6$ electrolyte. In the 1st cycle, the irreversible peak oxidation of the monomer has an onset at 770 mV. Two very small reduction peaks at ca. 605 mV and 270 mV (which are much more evident in the 50th cycle) on the back-sweep are indicative of the reduction of the initially deposited polymer. Films of polymerized C6DTP (pC6DTP) were formed by substituting the Pt button working electrode with ITO-coated glass slides. Electropolymerizing the monomer at +1000 mV (vs. Ag/AgCl) for 150 sec resulted in a thick adherent dark-blue films that was measured to be 977±116 nm thick films after storing in a 35 °C vacuum oven for 24 hours. These films were conditioned prior to running their cyclic voltammograms by repeatedly cycling them in a monomer-free solution of ACN / 0.1 M $TBAPF_6$. These cyclic voltammograms were run from -500 mV to 900 mV (100 mV/s) (cf. **Figure 2b**) and indicate the reversibility of the oxidation process of the pC6DTP films by the re-tracings of the cyclic runs. This suggests that no electrochemical degradation has taken place and the onset of the oxidation potential can be related to the ionization potential (IP). The onset potential (E_o) was estimated from the intersection of the two tangents drawn at the rising oxidation current and background current to give a value of 225 mV. Referring the potential value to the standard hydrogen electrode (SHE) and in turn to the vacuum level reference, the ionizing potential is estimated through $IP(eV) = e(E_o + 4.4)$, giving an IP for pC6DTP of 4.63 eV[41, 42]. Readily oxidizedable conjugated polymers are characterized by IP values under 5 eV, such as poly(pyrrole) and poly(1,3-ethylenedioxythiophene), which are more stable in their poly(cationic) (doped) state than in their neutral state at ambient conditions[43]. For comparison,

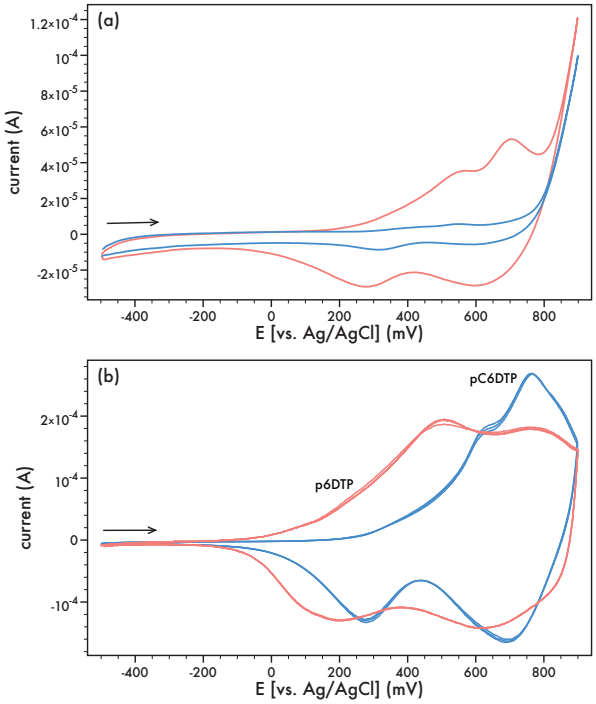

Figure 2: Cyclic voltammograms for the oxidation of **(a)** C6DTP monomer (c = 6.7 mM) in ACN / 0.1 M $TBAPF_6$; 1st cycle (blue) and 50th cycle (red). **(b)** pC6DTP (blue) and p6DTP (red). Electrolyte was ACN / 0.1 M $TBAPF_6$ and scan rate was 100 mV/s.

the cyclic voltammograms of poly(4-(6-hexyl)-4H-dithieno[3,2-b:2',3'-d]pyrrole) (p6DTP) is presented in **Figure 2b**. The repeat unit of this polymer is mirrored in pC6DTP but without the pendant carbazole ring. The IP of p6DTP is 4.4 eV, a value similar to reported energy levels in some N-substituted alkyl and alkyl ether polyDTPs[25, 44], and indicates that the oxidation of p6DTP is easier than pC6DTP. It is plausible the electron-accepting carbazole moieties of pC6DTP lowers the polymer's HOMO level even though its attached to the polymer backbone through a 6-carbon alkyl chain.

Scanning the films up to +1500 mV (cf. ESI) resulted in the appearance of an additional oxidation peak ascribed to the carbazoyl moiety, although the overlapping characteristics of the peaks made it difficult to make a structural assignment. Nonetheless, performing a cyclic voltammogram on the small molecule 9H-carbazole in the same conditions (10 mM in ACN / 0.1 M $TBAPF_6$) (cf. ESI) resulted in an oxidation onset of 1125 mV, indicating an IP of 5.53 eV[45], a value similar to the IP value of 5.52 eV for the non-conjugated polymer 2-(9H-carbazol-9-

yl)ethyl methacrylate[46].

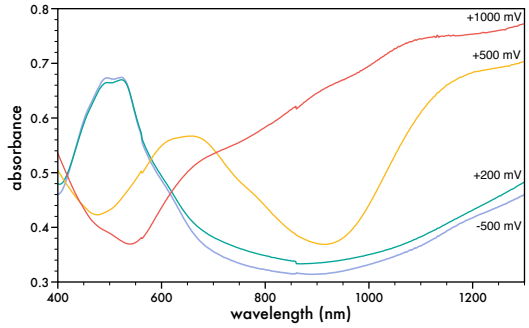

Figure 3: UV-Vis-NIR spectra obtained from spectroelectrochemical investigation of pC6DTP films. Applied voltages are referenced vs. Ag/AgCl.

The UV/Vis-NIR spectrochemical properties of the 977 nm thick pC6DTP films are presented in **Figure 3**. These spectra are typical of a conjugated polymer that is undergoing oxidative doping. The neutral polymer at -500 mV exhibits a peak ca. 505 nm that diminishes with increasing positive voltage on the working electrode and the appearance & growth of a peak at 644 nm (+500 mV) that is ascribed to the formation of localized positive polarons (radical cation). This peak disappears with increasing voltage (+1000 mV) on the working electrode as the polarons recombine into delocalized bipolarons, resulting in a featureless absorption tail that extends from 550 nm out to 1300 nm of the spectra (cf. **Figure 3**). The absorbance peak of the neutral polymer has an onset at 700 nm, giving pC6DTP an electronic bandgap of 1.77 eV, similar to values for N-substituted alkyl polyDTPs[24, 37, 44]. Coupling the bandgap with the cyclic voltammogram derived HOMO value results in a LUMO energy level for pC6DTP of 2.86 eV. Similarly, assuming that the 6-carbon alkyl spacer between the carbazole and the polymer backbone diminishes the intra- and/or inter-chain electronic interactions, the UV/Vis-NIR characteristics of the small molecule 9H-carbazole indicate that the carbazole's band gap is approximately 3.58 eV, which when coupled with the cyclic voltammogram derived HOMO value, gives a LUMO value of 1.98 eV.

The electrical properties of pC6DTP were investigated by initially electropolymerizing the polymer onto ITO coated glass slides. These films were then cycled repeatedly from -500 mV to + 900 mV (vs. Ag/AgCl) in monomer-free ACN / 0.1 M $TBAPF_6$ solution to fully polymerize any remaining monomer or oligomers in the film, and then exposed to +1000 mV for 60 secs to fully oxidize and dope the films ($pC6DTP_{ox}$). These films were then rinsed with deionized water and stored in a vacuum oven at 35 °C for 24 hours, after which, a 200 nm thick aluminum electrode was evaporated over the 247±22 nm film to form an ITO/$pC6DTP_{ox}$/Al device. The energy levels in the device structure ITO/$pC6DTP_{ox}$/Al as well as 9H-carbazole are presented in **Figure 4**. To establish the dc current–voltage (I-V) characteristic of $pC6DTP_{ox}$, the devices were subjected to a continuously varying dc voltage from ±4V which resulted in an erratic non-recursive I-V response. A signature characteristic exhibited by an "ideal" memristor is that they do not exhibit a predictable dc I-V curve since the device is never in equilibrium with their source[47]. There have been numerous examples of memristive systems in the literature that have presented continuously varying dc I-V curves as the dc voltage is tuned over a defined voltage interval[48].

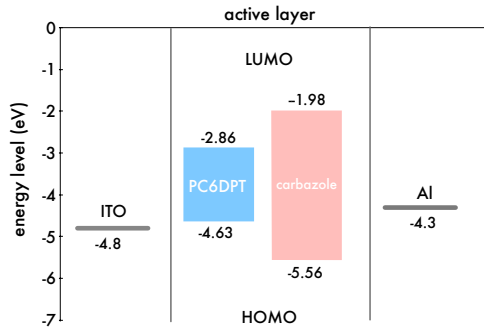

Figure 4: Electronic characteristics of neutral pC6DPT measured by UV-vis spectroscopy and cyclovoltammetry; all energies expressed in eV and are relative to the vacuum level. LUMO values are based on the difference of the measured oxidation potential (HOMO) and the energy at the experimentally observed electronic absorption band edge. The experimentally derived HOMO/LUMO energy values of 9H-carbazole (carbazole) are presented for reference purposes.

The voltage history-dependent current response makes it challenging to simply assess the level of dc conductivity of the device. To that end, **Figure 5** presents the dc I-V response of a $pC6DTP_{ox}$ device to $3x10^4$ stochastic voltage pulses. The ITO/$pC6DTP_{ox}$/Al device had the ITO electrode tied to ground and a square-wave voltage pulse of 67 ms duration and with a magnitude randomly selected from a uniform distribution scaled between ±4V was applied to the aluminum electrode. The resulting I-V curve defines an envelope of possible current responses from an applied dc potential without the history dependance between successive voltage impulses and spans the current range from 1 nA to 10 μA over the ±4V range. In comparison, **Figure 5** presents

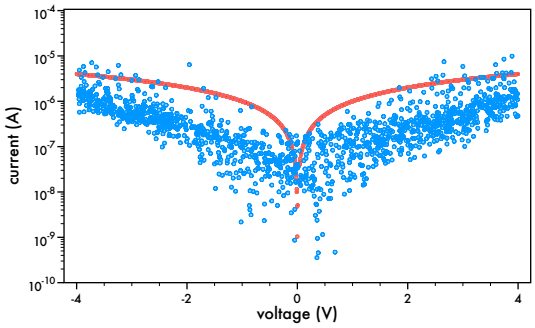

Figure 5: Conductance of pC6DTP$_{ox}$ device (blue) with random excitatory voltage pulses. Device was ITO/pC6DTP$_{ox}$/Al and was measured at 23 °C. Stochastic voltage-current relationship of 1 MΩ standard resistor (red) is also presented.

the corresponding I-V response of a 1 MΩ standard resistor that was exposed to the same stochastic voltage pulses. As expected, the standard resistor has a current response that is predictable even when excited with stochastic voltage pulses.

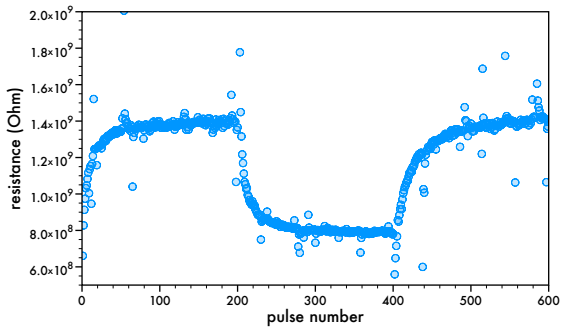

Figure 6: The voltage-pulse train response of a ITO/pC6DTP$_{ox}$/Al device.

The voltage-pulse train response of a pC6DTP$_{ox}$-based device to a number of consecutive pulses was studied in order to assess the saturation effects of the device. **Figure 6** presents the resistance of a pC6DTP$_{ox}$ device with 200 sequential pulses with magnitude of ±500 mV. A singular pulse was 67 ms in duration and was followed 124 ms later by a 50 mV measuring pulse. The pulses repeated every 610 ms. In the initial +500 mV biased pulse train, the resulting resistance response in the device was a gradual increase from 8x10^8 Ω to a saturated value of 1.4x10^9 Ω, a 75% increase. Pulsing the device with more than 200 consecutive pulses did not appreciably increase the resistance. Reversing the polarity and pulsing the device with -500 mV$_{DC}$ train resulted in the gradual drop in resistance back to the starting value of 8x10^8 Ω. The device is clearly exhibiting a response very similar in form to long-term potentiation (LTP) and long-term depression (LTD) seen in synapses in biological systems[49]. In the neurosciences, LTP and LPD are enduring changes in synaptic strength, induced by specific patterns of synaptic activity, that have received much attention as cellular models of information storage in the central nervous system[50–52].

In order to explain the ability of pC6DTP$_{ox}$ to alter its conductivity with voltage pulses, one has to inspect initially the alignment of the experimentally derived energy levels in the neutral pC6DTP device (cf. **Figure 4**). The energy difference between the HOMO (-4.63 eV) and LUMO (-2.86 eV) of pC6DTP and the work function of the metal electrodes (ITO = -4.8 eV[53], Al = -4.3 eV) will result in Schottky barriers being formed at both interfaces[54]. In this diagram, the depicted energy profile of pC6DTP is representative of the neutral polymer. Assuming that the change in the pC6DTP bandstructure with oxidation would be similar to polypyrrole[55], the formation of bipolaron bands (as indicated in the **Figure 3**), would shift the HOMO level more negative (verified in subsequent density functional calculations (DFT)). In this scenario, the ITO electrode presents a better vacuum level alignment with pC6DTP$_{ox}$, such that the transport is controlled by the injection barrier, making this structure predominately a hole transporting device.

One of the fundamental characteristics of synaptic plasticity in biological neural networks is spike-timing-dependent-plasticity (STDP)[56]. Replication of STDP in a synthetic model is critical for emulating biological systems[57, 58]. STDP can be interpreted as a spike-based form of a Hebbian learning rule where the efficacy of interneuronal connections is modulated by the relative timing of the output and input spikes (action potentials) to the neurons[59]. In general, a presynaptic spike that precedes a postsynaptic spike within a defined time period leads to LTP while LTD is observed if there is a reversal of the timing order of the spikes. The degree of change in synaptic strength is a function of the time differential between the pre- and postsynaptic spikes in both cases and elevated changes are correlated to short time differentials. STDP has been demonstrated in multiple mammalian species, including humans, and is considered the basis for cognitive learning[59, 60].

The STDP response of an ITO/pC6DTP$_{ox}$/Al memristor is presented in **Figure 7** where the ITO

and aluminum electrodes were designated the presynaptic and postsynaptic neuron, respectively, and the device was exposed to presynaptic and postsynaptic spike pairs with differing time intervals. Using presynaptic and postsynaptic spikes with a voltage profile that was a 500 mV magnitude square wave of 50 ms duration, the potentiation and depression of the synaptic weight could be modulated with a variation in the timing offset (δt) of the two pulses. In this study, the device was presented with a timing offset that was randomly selected from a uniform distribution to insure that the resulting current response of the device was not correlated to the previous timing offset run. The measuring pulse was a 50 mV magnitude square wave of 50 ms duration that initiated 50 ms after the last pre- or postsynaptic spike terminated while the weighting factor (ΔW) was determined from the current values of the device, scaled between -1 and 1, for the 1x10^3 spike-pair sampling run. In **Figure 7**, when the presynaptic spike arrives before the postsynaptic spike ($\delta t > 0$), there is a potentiation of the synaptic weight (ΔW) while depression occurs when the presynaptic spike arrives after the postsynaptic spike ($\delta t < 0$). This response is similar to a Asymmetric Hebbian Learning Rule, where $\delta t > 0$ leads to long-term potentiation (LTP) of the synapse and $\delta t < 0$ leads to long-term depression (LTD) of the synapse[59, 60].

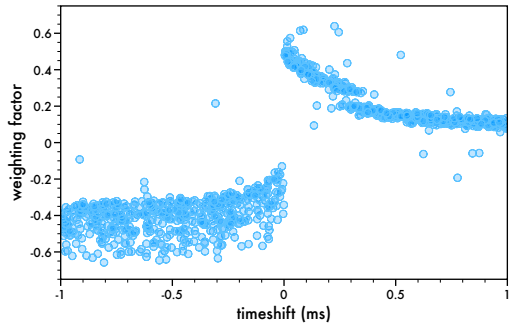

Figure 7: Spike-timing-dependent-plasticity (STDP) of ITO/pC6DTP$_{ox}$/Al memristor.

The voltage-pulse train response of a pC6DTP$_{ox}$-based device to a number of linear-increasing or decreasing voltage pulses was studied in order to assess the ability of the device to track its voltage history through resistivity modulations. **Figure 8** presents the applied voltage profile to a pC6DTP$_{ox}$ device and its resulting resistance. The voltage profile was a square wave pulse of 50 ms width with a linear increasing or decreasing magnitude, ranging from 250

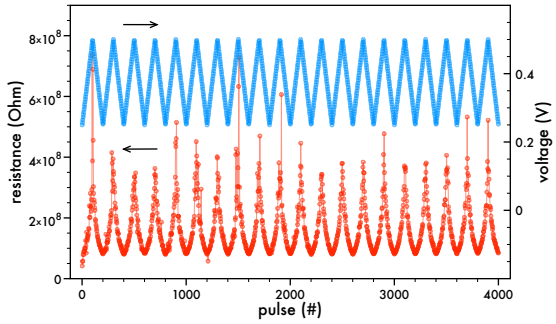

Figure 8: The linear-increasing or decreasing voltage pulse response of a ITO/pC6DTP$_{ox}$/Al memristor.

mV to 500 mV, with 50 mV magnitude measuring pulse 50 ms after the resistivity modulation pulse. The device is clearly capable of tracking an ascending and descending voltage pulse stream and appears to exhibit larger changes in resistivity with greater voltage magnitudes. This continuous change allows for the device to gradually change its learning rate with the increasing/decreasing pulsing and is closer in performance to biological plasticity data[61]. It should be emphasized that the device exhibits *increases* in resistivity with positive voltage impulses that are less than ca. +1000 mV in magnitude. Exceeding this value results in the device exhibiting a *decrease* in resistivity with positive voltage impulses. Though, at the present time, its unclear what mechanism is operative that results in an *increase* in the device resistivity with the positive voltage pulses, this "negative resistance" behavior has been observed in molecular electronics[62, 63] and is the basis for commercial electronic components[64]. Similar to the pC6DTP$_{ox}$ device, these previously studied systems only exhibit a negative resistance behavior over a limited portion of their voltage or current range[62–64]. Further understanding of the underlying mechanism and experimentation with various ligands should allow us to identify the key chemical/structural traits for this behavior.

The volatility of the resistivity modulations are presented in **Figure 9**, where a linear voltage pulse ramp from 0 mV to 200 mV and the corresponding device resistivity is presented. In this case, when the last impulse of 200 mV is applied to the device at ca. 41.5 secs, 50 mV voltage read pulses continue to be executed every 0.5 sec for another 45 secs. Within 6 secs after the cessation of the linear-increasing voltage pulses, the resistivity of the device has dropped by 10% of its maximum modulated value, though this

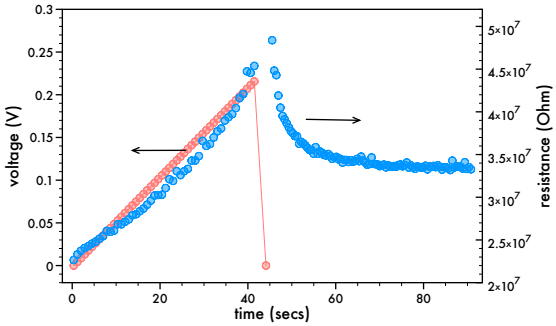

Figure 9: Decay response of a ITO/pC6DTP$_{ox}$/Al memristor after the cessation of a linear-increasing voltage pulse train.

decay is quickly halted and the resistivity plateaus to a value that is 76% of its maximum modulated value within ca. 24 secs. At room temperature, one could expect the molecular "structure" that is achieved with the voltages pulses and results in an increase in device resistivity to thermalize and relax to a state that has a lower resistivity with the cessation of the voltage pulses[65].

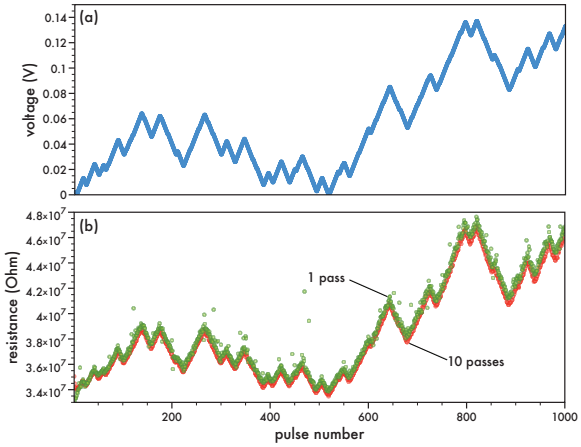

Figure 10: Voltage profile and resistance change with a "random" voltage profile applied to ITO/pC6DTP$_{ox}$/Al memristor. Single run (green) and 10-cycle average value (red).

Based on **Figures 8-10**, it appears that the pC6DTP$_{ox}$ device is capable of tracking voltage pulse streams, through resistivity modulations, that are "predictable", i.e. constant or linearly increasing/decreasing magnitudes. It was unclear what a random voltage pulse stream would do to the resistivity modulations. **Figure 10** presents the resistance response of a pC6DTP$_{ox}$ device to an arbitrary-generated potential profile. A potential profile was generated as a random walk between 0 mV and 200 mV in 1 mV increments and stored (cf. **Figure 10a**). The device was then subjected to this potential profile in the form of a 67 ms long square wave pulse with a magnitude corresponding to a value stored in the potential profile (cf. **Figure 10a**), with the pulses being spaced 860 ms apart. A measuring 50 mV square wave pulse with 160 ms width was initiated 127 ms after the potential profile pulse. The corresponding resistance is presented in **Figure 10b** where the device was subjected to the same potential profile a number of times to assess the reproducibility of the response. In **Figure 10b**, the resistance response of the device to a single pass and the average response for 10 unique passes are presented. For the single pass, the resistance response tracked the potential profile with an occasional large deviation due to a stochastic current response, while the large spurious resistance values of the single pass were absent when the device was exposed to the potential profile in 10 recursive cycles and the measured resistance was averaged. Besides being subjected to the same potential profile a number of times to assess the reproducibility of the response, the device was cycled through differing voltage profiles (cf. ESI). Specifically, cycling through voltage profiles that alternated from non-zero magnitudes to all zero magnitudes always resulted in resistance responses that tracked the voltage profile.

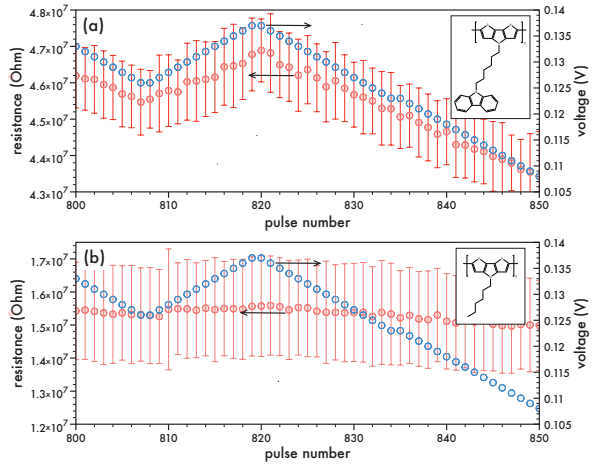

Figure 11: Average resistance response (red) with an applied potential profile (blue) with 1 mV increment of **(a)** pC6DTP$_{ox}$ and **(b)** p6DTP$_{ox}$ device. Device was subjected to same voltage profile 10 times and error bars represent standard deviation from mean. Inset presents structure of polymer repeat unit.

The voltage magnitudes and energy requirements to trigger a synaptic event is an important consideration

in the design of an artificial synapse. The consecutive changes in the resistance (synaptic event) for the pC6DTP$_{ox}$ device was accomplished by a 1 mV pulse of 67 ms in duration; a voltage magnitude comparable to a recently proposed three-terminal electrochemical low-voltage artificial synapse based on PEDOT:PSS[19]. Similarly, biological neuromorphic systems achieve energy consumption per operation that is an extremely small amount of energy, on the order of 1-10 fJ per synaptic event. For three-terminal artificial synapses based on conjugated polymers, the energy consumption has been reduced to the femtoJoule level[19, 66], while most two-terminal artificial synapses based on conjugated polymers presented in the literature have energy costs over 100 pJ per event[67, 68]. An electronic synapses has an energy consumption calculated by measuring the current that flows through the device during a resistance altering pulse and in the current case, the energy consumed to program the device is determined to be ca. 100 fJ (E $= V \times i \times t =$ 1 mV x 1.5 nA x 67 ms), a value an order of magnitude greater than a biological system but significantly less than previously published two-terminal devices.

Figure 11 presents a close-up of the applied potential profile and corresponding average resistance values with standard deviation for the 10-cycle on the pC6DTP$_{ox}$ device. In addition, **Figure 11** presents the 10-cycle average response of a device composed of p6DTP$_{ox}$, the structurally similar polymer to pC6DTP that does not contain a pendant carbazoyl moiety. Unlike pC6DTP$_{ox}$, this latter polymer (p6DTP$_{ox}$), did not track the voltage profile, though it was clearly electrically conductive.

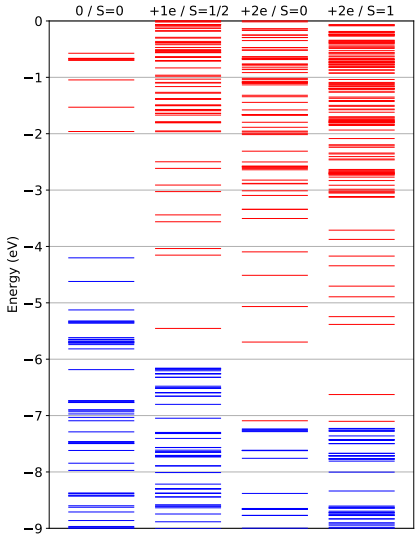

Figure 12: Orbital energy levels of a pC6DTP pentamer in the q=0 ($M = 1$), q=+1e ($M = 2$), q=+2e ($M = 1$), and q=+2e ($M = 3$) state. Occupied electronic levels are blue while empty electronic levels are red. DFT calculations with B3LYP/6-31G* theory.

The presence of the carbazoyl moiety in pC6DTP$_{ox}$ relative to p6DTP$_{ox}$ was the only structural difference between the polymers and the ability to modulate the resistivity existed only for pC6DTP$_{ox}$. We speculate that the carbazoyl moiety must be involved in charge transfer in the oxidized ground state of pC6DTP even though, in the neutral state, hole mobility would be improbable from the backbone to the ligand due to their 0.93 eV difference (cf. **Figure 4**). In our testing configuration, the polymer films are oxidized and exhibit bipolaronic states (cf. **Figure 3**) and its well established that oxidized conjugated polymers have shifted orbital energy states relative to the neutral polymer and this phenomena could be a contributing factor on the discrepancies in the electrical response between pC6DTP$_{ox}$ and p6DTP$_{ox}$.

To investigate this possibility, the orbital energy states of a pentamer of pC6DTP were calculated using density functional theory (DFT) with the 6-31G* basis set at various oxidation levels. The DFT approach utilized the three-parameter hybrid exchange functional of Beckel and the Lee-Yang-Parr correlation functional (B3LYP)[69]. The degree of polymerization of the polymer can have a marked effect in the calculated energies though experimental and theoretical studies indicate that saturation effects occur quickly by 4-6 repeat units[70–72]. In the present case, a 6-mer and 5-mer exhibited similar energies and a pentamer (5-mer) was considered sufficiently long enough to approximate the saturation characteristics of an infinite chain. The orbital energies of the pentamer were calculated at the charged states of $q = 0, +1e$, and $+2e$. CV studies on N-alkyl substituted DPT polymers indicated that the polymer can reversibly exchange 0.6 electrons per monomer[37]. A 2^+ charge on the polymer would define the first bipolaron state of the oxidized ground-state pentamer, while the 1^+ charged singlet would define the first polaronic state[73]. For the bipolaronic state of $q = +2e$, the total spin can be 0 or 1, giving spin multiplicities ($M = 2S + 1$) of a singlet ($M = 1$) or triplet ($M = 3$). **Figure 12** presents the orbital energy diagram for the neutral and charged pC6DTP pentamer, while **Figure 13** presents the molecular orbitals (MO) for select energies. In **Figure 12**, the

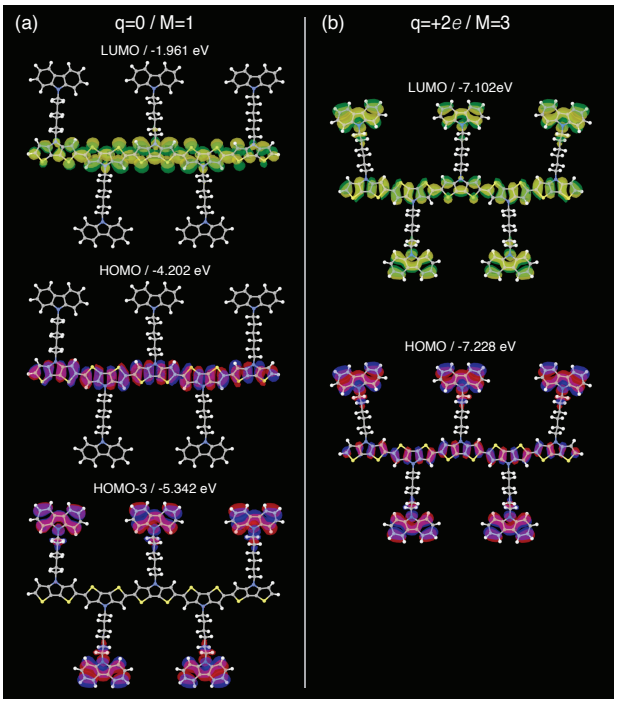

Figure 13: Molecular orbitals of pC6DTP pentamer: **(a)** q=0 (M=1) and **(b)** q=+2e (M=3) state. DFT calculations with B3LYP/6-31G* theory.

neutral pentamer exhibits a calculated LUMO energy (-1.961 eV) which is significantly closer (ca. 1 eV) to the vacuum level relative to experimental results (cf. **Figure 4**), a common issue with DFT when calculating virtual MOs[71]. The corresponding calculated HOMO energy value (-4.202 eV) is +0.4 eV from the experimentally determined value for the neutral polymer. The MOs for the HOMO and LUMO energies (cf. **Figure 13a**) indicate the orbitals for these two energy levels are localized on the chain backbone, while the MOs centered on the carbazoyl moieties are located in five degenerate energy states that are labeled HOMO-3 and are located at ca. -5.342 eV in **Figures 12**. The calculated orbital energy level for HOMO-3 is surprisingly close to the experimentally derived HOMO energy level (-5.56 eV) of the small molecule 9H-carbazole (cf. **Figure 4**). The MOs between the HOMO and HOMO-3 energy states are localized on the chain backbone. The energy difference between the HOMO and HOMO-3 energy states is ca. 1.14 eV, indicating a very low likelihood that these MOs would participate in charge transfer between these energy levels.

In contrast, **Figure 12** presents the energy diagram for the first polaronic state ($q = +1e$) with total spin $S = 1/2$ ($M = 2$) and first bipolaronic state ($q = +2e$) at spin multiplicities in the singlet ($M = 1$) or triplet ($M = 3$) state for the pC6DTP pentamer and indicates that the HOMO and LUMO energies have shifted away from the vacuum level for these charged species. The HOMO energy (-6.172 eV) of the polaronic state is significantly higher than both the bipolaronic energy states. In these calculations, the HOMO level (-7.228 eV) of the triplet state is ca. 0.01 eV lower than the HOMO level (-7.238 eV) of the singlet state, though the MO characteristics were similar for both spin multiplicities[73]. The doping procedure for the pC6DTP$_{ox}$ devices coupled with the appearance of delocalized bipolaron absorption bands in the UV-Vis-NIR spectra of the pC6DTP$_{ox}$ films (cf. **Figure 3**) confirms an abundance of bipolaronic energy states. For the triplet state, the MOs associated with both the LUMO and HOMO energy levels are now centered on the polymer backbone and carbazoyl moieties (cf. **Figure 13b**) suggesting that the pendant rings could participate in charge transfer between the backbone when the polymer is in a bipolaronic state. In this case, the molecular orbitals associated with these energy levels would need to be spatially adjacent whereby charge transfer could occur.

Based on the DFT results, we can imagine there are two independent but synergistic paths to achieving electrical percolation in the oxidized polymer whereby the chain backbone defines the main percolative path with the conformationally flexible pendant carbazole rings offering fine changes in conductive cluster size and resulting bulk conductivity by moving towards or away from the backbone of the chain under an imposed electric field. These results could offer an explanation why p6DTP, the structurally similar polymer to pC6DTP except for the lack of carbazole rings, does not exhibit the multiple resistive states that the oxidized form of pC6DTP does.

3 Conclusion

A newly synthesized hybrid conjugated polymer with pendant carbazole rings, that is, poly(4-(6-(9H-carbazol-9-yl)hexyl)-4H-dithieno[3,2-b:2',3'-d]pyrrole) (pC6DTP), was employed in the fabrication of a two-terminal memristor with a Al/pC6DTP/ITO configuration where the polymer was electrochemicaly doped. Signature biological

synaptic responses to voltage spikes were demonstrated, such as potentiation & depression and spike timing dependent plasticity. The device was able to be programed through a 1 mV pulse, requiring only 100 fJ of energy, an energy value an order of magnitude greater than a biological synapse but significantly lower than current conjugated polymer-based two-terminal neomorphic emulating memristors. DFT studies on a pentamer of the polymer indicate that in the first bipolaronic state ($q = +2e$), the HOMO and LUMO energies have shifted away from the vacuum level relative to the neutral polymer and the MOs associated with both the LUMO and HOMO energy levels are now centered on the polymer backbone and carbazole moieties, offering a path for hole transport to/from the pendant group to the chain backbone. The charge transport along both the chain backbone and pendant rings was responsible for the ability of the polymer to exhibit a multitude of resistive states through a synergistic double percolation route.

4 Acknowledgments

The authors thank the Gregg-Graniteville Foundation and the National Science Foundation (OIA-1632881 & OIA-1655740) and the Ministry of Education, Youth and Sports of the Czech Republic – Program INTER-EXCELLENCE (LTAUSA19066) and DKRVO (RP/CPC/2021/006) for financial support.

5 Experimental

5.1 Materials and methods

All reagents were purchased from Alfa Aesar, TCI America, and used without further purification. All the solvents used for reactions were distilled under argon after drying over an appropriate drying reagent. ^{1}H and ^{13}C NMR spectra were recorded on a JEOL ECX–300 spectrometer. Chemical shifts for protons are reported in parts per million downfield from tetramethylsilane and are referenced to residual protium in the NMR solvent ($CDCl_3$: δ 7.26 ppm). Chemical shifts for carbons are reported in parts per million downfield from tetramethylsilane and are referenced to the carbon resonances of the solvent ($CDCl_3$: δ 77.16 ppm). Melting points were determined on EZ-Melt automated melting point apparatus. High resolution mass analysis was prepared using Waters Q-Tof Premier mass spectrometer.

5.2 Synthesis

1-azido-6-chlorohexane was synthesized according to the literature[74].

9-(6-azidohexyl)-9H-carbazole (1). Carbazole (1 g, 5.98 mmol) was dissolved in dry dimethylformamide (10 ml), then sodium hydride (0.16 g, 6.58 mmol) was added under nitrogen. Mixture was stirred at room temperature for 10 min., then 1-azido-6-chlorohexane (1.06 g, 6.58 mmol) was added. Obtained mixture was stirred and heated to 80 °C and kept at this temperature for 2 hours. After cooling, mixture was extracted with dichloromethane and washed with water three times. Organic solution was dried with Na2SO4, filtered and evaporated under vacuum. Crude product (95% pure by NMR) was used in the next step without additional purification. Yield 1.7 g (95%), pale brown oil.

^{1}H NMR ($CDCl_3$, δ, ppm): 1.37 (m, 4H), 1.52 (m, 2H), 1.86 (m, 2H), 3.18 (t, 2H, J=7.2 Hz), 4.28 (t, 2H, J=7.2 Hz), 7.22 (m, 2H, J=6.9 Hz, J=7.9 Hz), 7.36-7.47 (m, 4H, J=6.9 Hz, J=7.9 Hz), 8.08 (d, 2H, J=7.9 Hz).

6-(9H-carbazol-9-yl)hexan-1-amine (2). 9-(6-azidohexyl)-9H-carbazole (1.6 g, 5.47 mmol) and triphenylphosphine (1.83 g, 6.98 mmol) were dissolved in tetrahydrofuran (20 ml). Solution was stirred at room temperature for 24 h. Water (1 ml) was added into solution and stirred for additional 30 minutes. Solvent was evaporated under vacuum. The residue was dissolved in methanol (10 ml) and acidified by solution of HCl in methanol. Obtained mixture was evaporated under vacuum, mixed with water (20 ml) and centrifuged to remove insoluble triphenylphosphine oxide. Water solution of hydrochloric salt of product was basidified with NaOH and extracted with diethyl ether twice. Organic solution was evaporated and crude product was purified by column chromatography. First solvent – dichloromethane (to wash out impurities), second solvent – dichloromethane/methanol (3/1) with 2.5% of NH4OH (29% water solution) to wash out the product. Obtained amine reacts with CO2 from atmosphere and creates carbamates, has to be stored under nitrogen. Yield 1.3 g (89%), pale yellow oil.

^{1}H NMR ($CDCl_3$, δ, ppm): 1.40 (m, 6H), 1.87 (m, 2H), 2.21 (br.s, 2H, NH2), 2.66 (t, 2H, J=6.9 Hz),

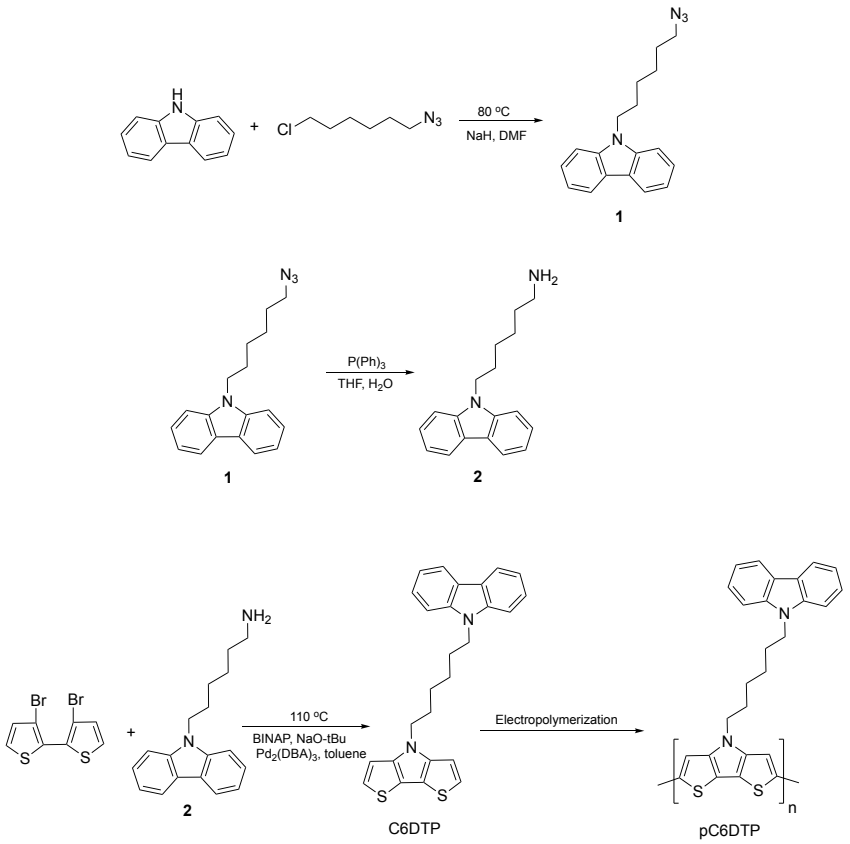

Figure 14: Synthetic route.

4.29 (t, 2H, J=6.9 Hz), 7.23 (m, 2H, J=6.9 Hz, J=7.9 Hz), 7.39-7.49 (m, 4H, J=6.9 Hz, J=7.9 Hz), 8.10 (d, 2H, J=7.9 Hz).

4-(6-(9H-carbazol-9-yl)hexyl)-4H-dithieno[3,2-b:2',3'-d]pyrrole (C6DPT) was prepared using palladium-catalysed Buchwald–Hartwig amination[75]. 3,3'-Dibromo-2,2'-bithiophene (0.3 g, 0.93 mmol), BINAP (0.06 g, 0.093 mmol), $Pd_2(dba)_3$ (0.015 g, 0.016 mmol), 6-(9H-carbazol-9-yl)hexan-1-amine (0.27 g, 1.02 mmol) and sodium tert-butoxide (0.22 g, 2.32 mmol) were mixed with dry toluene (10 ml) under nitrogen atmosphere. Obtained mixture was refluxed and stirred for 16 hours. After cooling, the mixture was extracted with diethyl ether, washed with water. Organic solution was dried with Na_2SO_4, filtered and evaporated under vacuum. The residue was purified by column chromatography. Solvent dichloromethane/hexane (1/2), Rf=0.3. Yield 0.3 g (75%), clear solid, m.p=108 °C.

^{1}H NMR ($CDCl_3$, δ, ppm): 1.29 (m, 4H), 1.77 (m, 4H), 4.07 (t, 2H, J=6.5 Hz), 4.21 (t, 2H, J=7.2 Hz), 6.85 (d, 2H, J=5.5 Hz), 7.06 (d, 2H, J=5.5 Hz), 7.21 (m, 2H, J=1.0 Hz, J=7.9 Hz), 7.31 (d, 2H, J=7.9 Hz), 7.43 (m, 2H, J=1.0 Hz, J=7.9 Hz0, 8.08 (d, 2H, J=7.9 Hz).

^{13}C NMR (CDCl3, δ, ppm): 26.8, 26.9, 28.9, 30.2, 42.8, 47.1, 108.7, 110.9, 114.7, 118.9, 120.5, 122.8, 122.9, 125.7, 140.2, 144.9.

HRMS (m/z): calc. for $C_{26}H_{24}N_2S_2$, 428.14; found, 428.14.

5.3 Electropolymerization

Cyclovoltammetry (CV) was performed with a BASi 100A Electrochemical Analyzer coupled to a C3 Cell Stand. To investigate the CV characteristics of the monomer C6DTP, 7.5 ml of a CH_3CN (ACN) solution containing 6.7 mM of the monomer and 0.1 M of $TBAPF_6$ was purged with nitrogen for 20 min before a 3-electrode configuration with Ag/AgCl reference electrode, Pt wire counter electrode, and Pt button electrode were cycled from -0.5 V to 0.9 V (vs. Ag/AgCl) at a scan rate of 0.1 V/s. To investigate

the electrochemical characteristics of pC6DTP, the Pt button electrode was replaced with ITO coated glass slides to form polymer films on the electrodes. CV scans of these polymer-coated electrodes were performed in monomer-free 100 mM ACN / $TBAPF_6$ solution from -0.5 V to 0.9 V (vs. Ag/AgCl) and at a scan rate of 0.1 V/s. ITO/pC6DTP$_{ox}$/Al device had 247.5±22.2 nm thick polymer film. Data presented in the IUPAC redox voltage and current convention (positive potential to the right of the graph; positive / oxidizing current at the top of the graph).

UV/Vis-NIR spectrochemical properties of the pC6DTP films on ITO were carried out in a 10 mm path-length quartz cuvette outfitted with a Ag/AgCl reference electrode and Pt wire counter electrode all immersed in a monomer-free 100 mM ACN / $TBAPF_6$ solution. An Ocean Optics PC2000 ISA Fiber Optic Spectrometer coupled to an Ocean Optics ISS-UV-VIS-2 illuminated cuvette holder were used to collect the spectra as the potential was varied by a BASi 100A Electrochemical Analyzer.

5.4 Electrical Characterization

The electrical studies were performed using an HP 4156A Semiconductor Parameter Analyzer coupled to a HP 16058A Test Fixture through triaxial leads and controlled by customized HTBasic v.10 code. For most measurements, unless stated otherwise, the ITO electrode was kept at zero potential via SMU3 while potentials were applied to the aluminum electrode via SMU1.

5.4.1 Long-term Potentiation (LTP) and Long-term Depression (LTD)

The voltage-pulse train response of a ITO/pC6DTP$_{ox}$/Al device was generated (cf. **Figure 6**) by applying a 500 mV in magnitude pulse to the aluminum electrode that was 67 ms in duration. This pulse was followed 124 ms later by a 50 mV measuring pulse of 162 ms duration that integrated the current for 16.7 ms. The modify & measure pulse sequence was repeated every 610 ms.

5.4.2 Spike-timing-dependent-plasticity (STDP)

The STDP response of a ITO/pC6DTP$_{ox}$/Al device was generated (cf. **Figure 7**) by applying a presynaptic and postsynaptic spike that was a 500 mV magnitude square wave with a 50 ms duration. The ITO and aluminum electrodes were designated the presynaptic and postsynaptic neuron, respectively. The timing offset (δt) of the two pulses was randomly selected from a uniform distribution. The measuring pulse was a 50 mV magnitude square wave of 50 ms duration that initiated 50 ms after the last pre- or postsynaptic spike terminated.

5.5 Electronic Structure Calculations

The geometry optimizations were accomplished using the Gaussian 09 package without imposing any constraints on initial structures. Neutral pC6DPT (q = 0) and p-doped pC6DPT (q = +1e, +2e) were optimized at the B3LYP/6-31G* level of DFT. Restricted (close-shell) spin was used in the calculations for neutral chains (q = 0) and chains with even numbers of electrons for the singlet state (with the spin multiplicity M = 1). For all other cases, the unrestricted (open-shell) spin calculations were performed.

References Cited

[1] D. B. Strukov, G. S. Snider, D. R. Stewart, and R. S. Williams. The missing memristor found. *Nature*, 453(7191):80–83, 2008.

[2] J. J. S. Yang, D. B. Strukov, and D. R. Stewart. Memristive devices for computing. *Nature Nanotechnology*, 8(1):13–24, 2013.

[3] A. Szymanski, D. C. Larson, and M. M. Labes. A temperature-independent conducting state in tetracene thin film. *Applied Physics Letters*, 14(3):88–90, 1969.

[4] Kevorkia.J, M. M. Labes, D. C. Larson, and D. C. Wu. Bistable switching in organic thin films. *Discussions of the Faraday Society*, (51):139, 1971.

[5] A. R. Elsharkawi and K. C. Kao. Switching and memory phenomena in anthracene thin-films. *Journal of Physics and Chemistry of Solids*, 38(1):95–96, 1977.

[6] Y. Segui, B. Ai, and H. Carchano. Switching in polystyrene films - transition from on to off state. *Journal of Applied Physics*, 47(1):140–143, 1976.

[7] C. W. Chu, J. Ouyang, H. H. Tseng, and Y. Yang. Organic donor-acceptor system exhibiting electrical bistability for use in memory devices. *Advanced Materials*, 17(11):1440–+, 2005.

[8] F. Verbakel, S. C. J. Meskers, and R. A. J. Janssen. Electronic memory effects in a sexithiophene-poly(ethylene oxide) block copolymer doped with nacl. combined diode and resistive switching behavior. *Chemistry of Materials*, 18(11):2707–2712, 2006.

[9] D. I. Son, J. H. Kim, D. H. Park, W. K. Choi, F. Li, J. H. Ham, and T. W. Kim. Nonvolatile flexible organic bistable devices fabricated utilizing cdse/zns nanoparticles embedded in a conducting poly n-vinylcarbazole polymer layer. *Nanotechnology*, 19(5), 2008.

[10] G. Liu, B. Zhang, Y. Chen, C. X. Zhu, L. J. Zeng, D. S. H. Chan, K. G. Neoh, J. N. Chen, and E. T. Kang. Electrical conductivity switching and memory effects in poly(n-vinylcarbazole) derivatives with pendant azobenzene chromophores and terminal electron acceptor moieties. *Journal of Materials Chemistry*, 21(16):6027–6033, 2011.

[11] Y. K. Fang, C. L. Liu, and W. C. Chen. New random copolymers with pendant carbazole donor and 1,3,4-oxadiazole acceptor for high performance memory device applications. *Journal of Materials Chemistry*, 21(13):4778–4786, 2011.

[12] G. Liu, Q. D. Ling, E. Y. H. Teo, C. X. Zhu, D. S. H. Chan, K. G. Neoh, and E. T. Kang. Electrical conductance tuning and bistable switching in poly(n-vinylcarbazole)-carbon nanotube composite films. *Acs Nano*, 3(7):1929–1937, 2009.

[13] B. Cho, T. W. Kim, S. Song, Y. Ji, M. Jo, H. Hwang, G. Y. Jung, and T. Lee. Rewritable switching of one diode-one resistor nonvolatile organic memory devices. *Advanced Materials*, 22(11):1228–+, 2010.

[14] H. J. Yen, C. S. Shan, L. Wang, P. Xu, M. Zhou, and H. L. Wang. Development of conjugated polymers for memory device applications. *Polymers*, 9(1), 2017.

[15] Doo Seok Jeong, Inho Kim, Martin Ziegler, and Hermann Kohlstedt. Towards artificial neurons and synapses: a materials point of view. *Rsc Advances*, 3(10):3169–3183, 2013.

[16] A. Thomas. Memristor-based neural networks. *Journal of Physics D-Applied Physics*, 46(9):12, 2013.

[17] Z. Y. Wang, L. Y. Wang, M. Nagai, L. H. Xie, M. D. Yi, and W. Huang. Nanoionics-enabled memristive devices: Strategies and materials for neuromorphic applications. *Advanced Electronic Materials*, 3(7), 2017.

[18] J. Schmidhuber. Deep learning in neural networks: An overview. *Neural Networks*, 61:85–117, 2015.

[19] Y. van de Burgt, E. Lubberman, E. J. Fuller, S. T. Keene, G. C. Faria, S. Agarwal, M. J. Marinella, A. A. Talin, and A. Salleo. A nonvolatile organic electrochemical device as a low-voltage artificial synapse for neuromorphic computing. *Nature Materials*, 16(4):414–+, 2017.

[20] Y. Chen, G. Liu, C. Wang, W. B. Zhang, R. W. Li, and L. X. Wang. Polymer memristor for information storage and neuromorphic applications. *Materials Horizons*, 1(5):489–506, 2014.

[21] Scott Kirkpatrick. Percolation and conduction. *Reviews of Modern Physics*, 45(4):574–588, 1973.

[22] S. H. Foulger. Reduced percolation thresholds of immiscible conductive blends. *Journal of Polymer Science Part B-Polymer Physics*, 37(15):1899–1910, 1999.

[23] Erjun Zhou, Qingshuo Wei, Shimpei Yamakawa, Yue Zhang, Keisuke Tajima, Chunhe Yang, and Kazuhito Hashimoto. Diketopyrrolopyrrole-based semiconducting polymer for photovoltaic device with photocurrent response wavelengths up to 1.1 mu m. *Macromolecules*, 43(2):821–826, 2010.

[24] K. Ogawa and S. C. Rasmussen. N-functionalized poly(dithieno 3,2-b : 2 ',3 '-d pyrrole)s: Highly fluorescent materials with reduced band gaps. *Macromolecules*, 39(5):1771–1778, 2006.

[25] Jared F. Mike, Lin Shao, Ju-Won Jeon, and Jodie L. Lutkenhaus. Charge storage in decyl- and 3,6,9-trioxadecyl-substituted poly(dithieno 3,2-b:2,3-d pyrrole) electrodes. *Macromolecules*, 47(1):79–88, 2014.

[26] Hacer Azak, Huseyin Bekir Yildiz, and Buket Bezgin Carbas. Synthesis and characterization of a new poly(dithieno (3,2-b: 2 ', 3 '-d) pyrrole) derivative conjugated polymer: Its electrochromic and biosensing applications. *Polymer*, 134:44–52, 2018.

[27] G. B. Lin, Y. K. Qin, Y. S. Guan, H. Xu, W. Xu, and D. B. Zhu. pi-conjugated dithieno 3,2-b:2 ',3 '-d pyrrole (dtp) oligomers for organic thin-film transistors. *Rsc Advances*, 6(6):4872–4876, 2016.

[28] Sean J. Evenson, Matthew J. Mumm, Konstantin I. Pokhodnya, and Seth C. Rasmussen. Highly fluorescent dithieno 3,2-b:2 ',3 '-d pyrrole-based materials: Synthesis, characterization, and oled device applications. *Macromolecules*, 44(4):835–841, 2011.

[29] Cheng Wang, Gang Liu, Yu Chen, Shanshan Liu, Qibin Chen, Runwei Li, and Bin Zhang. Dithienopyrrole-/benzodithiophene-based donor-acceptor polymers for memristor. *Chempluschem*, 79(9):1263–1270, 2014.

[30] S. L. Lim, Q. D. Ling, E. Y. H. Teo, C. X. Zhu, D. S. H. Chan, E. T. Kang, and K. G. Neoh. Conformation-induced electrical bistability in non-conjugated polymers with pendant carbazole moieties. *Chemistry of Materials*, 19(21):5148–5157, 2007.

[31] T. M. McFarlane, B. Zdyrko, Y. Bandera, D. Worley, O. Klep, M. Jurca, C. Tonkin, S. H. Foulger, J. Vilcakova, P. Saha, and J. Pfleger. Design rules for carbazole derivatized n-alkyl methacrylate polymeric memristors. *Journal of Materials Chemistry C*, 6(10):2533–2545, 2018.

[32] T. McFarlane, Y. Bandera, B. Grant, B. Zdyrko, S. H. Foulger, J. Vilcakova, P. Saha, and J. Pfleger. Carbazole derivatized n-alkyl methacrylate polymeric memristors as flexible synaptic substitutes. *Advanced Electronic Materials*, 6(6):8, 2020.

[33] G. Liu, D. J. Liaw, W. Y. Lee, Q. D. Ling, C. X. Zhu, D. S. H. Chan, E. T. Kang, and K. G. Neoh. Tristable electrical conductivity switching in a polyfluorene-diphenylpyridine copolymer with pendant carbazole groups. *Philosophical Transactions of the Royal Society a-Mathematical Physical and Engineering Sciences*, 367(1905):4203–4214, 2009.

[34] B. Zhang, Y. L. Liu, Y. Chen, K. G. Neoh, Y. X. Li, C. X. Zhu, E. S. Tok, and E. T. Kang. Nonvolatile rewritable memory effects in graphene oxide functionalized by conjugated polymer containing fluorene and carbazole units. *Chemistry-a European Journal*, 17(37):10304–10311, 2011.

[35] S. Park, T. J. Lee, D. M. Kim, J. C. Kim, K. Kim, W. Kwon, Y. G. Ko, H. Choi, T. Chang, and M. Ree. Electrical memory characteristics of a nondoped pi-conjugated polymer bearing carbazole moieties. *Journal of Physical Chemistry B*, 114(32):10294–10301, 2010.

[36] S. G. Hahm, N. G. Kang, W. Kwon, K. Kim, Y. G. Ko, S. Ahn, B. G. Kang, T. Chang, J. S. Lee, and M. Ree. Programmable bipolar and unipolar nonvolatile memory devices based on poly(2-(n-carbazolyl)ethyl methacrylate) end-capped with fullerene. *Advanced Materials*, 24(8):1062–1066, 2012.

[37] A. Berlin, G. Pagani, G. Zotti, and G. Schiavon. Electrochemical polymerization of 1h,7h-pyrrolo(2',3'-4,5)-thieno(3,2-b)pyrrole and 4h-dithieno(3,2-b-2',3'-d)pyrrole. *Makromolekulare Chemie-Macromolecular Chemistry and Physics*, 193(2):399–409, 1992.

[38] G. Zotti, G. Schiavon, A. Berlin, G. Fontana, and G. Pagani. Novel, highly conducting, and soluble polymers from anodic coupling of alkyl-substituted cyclopentadithiophene monomers. *Macromolecules*, 27(7):1938–1942, 1994.

[39] K. Ogawa and S. C. Rasmussen. A simple and efficient route to n-functionalized dithieno 3,2-b : 2 ',3 '-d pyrroles: Fused-ring building blocks for new conjugated polymeric systems. *Journal of Organic Chemistry*, 68(7):2921–2928, 2003.

[40] G. Koeckelberghs, L. De Cremer, W. Vanormelingen, W. Dehaen, T. Verbiest, A. Persoons, and C. Samyn. Improved synthesis of n-alkyl substituted dithieno 3,2-b : 2 ',3 '-d pyrroles. *Tetrahedron*, 61(3):687–691, 2005.

[41] L. Micaroni, F. C. Nart, and I. A. Hummelgen. Considerations about the electrochemical estimation of the ionization potential of conducting polymers. *Journal of Solid State Electrochemistry*, 7(1):55–59, 2002.

[42] C. M. Cardona, W. Li, A. E. Kaifer, D. Stockdale, and G. C. Bazan. Electrochemical considerations for determining absolute frontier orbital energy levels of conjugated polymers for solar cell applications. *Advanced Materials*, 23(20):2367–2371, 2011.

[43] P. Bujak, I. Kulszewicz-Bajer, M. Zagorska, V. Maurel, I. Wielgus, and A. Pron. Polymers for electronics and spintronics. *Chemical Society Reviews*, 42(23):8895–8999, 2013.

[44] S. Fortsch and P. Bauerle. Synthesis and characterization of two isomeric dithienopyrrole series and the corresponding electropolymers. *Polymer Chemistry*, 8(23):3586–3595, 2017.

[45] K. Karon and M. Lapkowski. Carbazole electrochemistry: a short review. *Journal of Solid State Electrochemistry*, 19(9):2601–2610, 2015.

[46] C. F. Huebner, V. Tsyalkovsky, Y. Bandera, M. K. Burdette, J. A. Shetzline, C. Tonkin, S. E. Creager, and S. H. Foulger. Nonvolatile optically-erased colloidal memristors. *Nanoscale*, 7(4):1270–1279, 2015.

[47] L. Chua. If it's pinched it's a memristor. *Semiconductor Science and Technology*, 29(10), 2014.

[48] S. P. Adhikari, M. P. Sah, H. Kim, and L. O. Chua. Three fingerprints of memristor. *Ieee Transactions on Circuits and Systems I-Regular Papers*, 60(11):3008–3021, 2013.

[49] T. V. P. Bliss and G. L. Collingridge. A synaptic model of memory - long-term potentiation in the hippocampus. *Nature*, 361(6407):31–39, 1993.

[50] R. C. Malenka and R. A. Nicoll. Neuroscience - long-term potentiation - a decade of progress? *Science*, 285(5435):1870–1874, 1999.

[51] R. C. Malenka and M. F. Bear. Ltp and ltd: An embarrassment of riches. *Neuron*, 44(1):5–21, 2004.

[52] J. L. McGaugh. Neuroscience - memory - a century of consolidation. *Science*, 287(5451):248–251, 2000.

[53] J. S. Kim, M. Granstrom, R. H. Friend, N. Johansson, W. R. Salaneck, R. Daik, W. J. Feast, and F. Cacialli. Indium-tin oxide treatments for single- and double-layer polymeric light-emitting diodes: The relation between the anode physical, chemical, and morphological properties and the device performance. *Journal of Applied Physics*, 84(12):6859–6870, 1998.

[54] Q. D. Ling, Y. Song, S. L. Lim, E. Y. H. Teo, Y. P. Tan, C. X. Zhu, D. S. H. Chan, D. L. Kwong, E. T. Kang, and K. G. Neoh. A dynamic random access memory based on a conjugated copolymer containing electron-donor and -acceptor moieties. *Angewandte Chemie-International Edition*, 45(18):2947–2951, 2006.

[55] J. L. Bredas and G. B. Street. Polarons, bipolarons, and solitons in conducting polymers. *Accounts of Chemical Research*, 18(10):309–315, 1985.

[56] L. F. Abbott and Sacha B. Nelson. Synaptic plasticity: taming the beast. *Nature Neuroscience*, 3(11):1178–1183, 2000.

[57] S. Z. Li, F. Zeng, C. Chen, H. Y. Liu, G. S. Tang, S. Gao, C. Song, Y. S. Lin, F. Pan, and D. Guo. Synaptic plasticity and learning behaviours mimicked through ag interface movement in an ag/conducting polymer/ta memristive system. *Journal of Materials Chemistry C*, 1(34):5292–5298, 2013.

[58] Y. Li, Y. P. Zhong, J. J. Zhang, L. Xu, Q. Wang, H. J. Sun, H. Tong, X. M. Cheng, and X. S. Miao. Activity-dependent synaptic plasticity of a chalcogenide electronic synapse for neuromorphic systems. *Scientific Reports*, 4, 2014.

[59] M. C. W. van Rossum, G. Q. Bi, and G. G. Turrigiano. Stable hebbian learning from spike timing-dependent plasticity. *Journal of Neuroscience*, 20(23):8812–8821, 2000.

[60] R. C. Froemke and Y. Dan. Spike-timing-dependent synaptic modification induced by natural spike trains. *Nature*, 416(6879):433–438, 2002.

[61] S. Song, K. D. Miller, and L. F. Abbott. Competitive hebbian learning through spike-timing-dependent synaptic plasticity. *Nature Neuroscience*, 3(9):919–926, 2000.

[62] J. Chen, M. A. Reed, A. M. Rawlett, and J. M. Tour. Large on-off ratios and negative differential resistance in a molecular electronic device. *Science*, 286(5444):1550–1552, 1999.

[63] J. Chen, W. Wang, M. A. Reed, A. M. Rawlett, D. W. Price, and J. M. Tour. Room-temperature negative differential resistance in nanoscale molecular junctions. *Applied Physics Letters*, 77(8):1224–1226, 2000.

[64] L. Esaki. New phenomenon in narrow germanium para-normal-junctions. *Physical Review*, 109(2):603–604, 1958.

[65] Z. J. Donhauser, B. A. Mantooth, K. F. Kelly, L. A. Bumm, J. D. Monnell, J. J. Stapleton, D. W. Price, A. M. Rawlett, D. L. Allara, J. M. Tour, and P. S. Weiss. Conductance switching in single molecules through conformational changes. *Science*, 292(5525):2303–2307, 2001.

[66] W. Xu, S. Y. Min, H. Hwang, and T. W. Lee. Organic core-sheath nanowire artificial synapses with femtojoule energy consumption. *Science Advances*, 2(6):7, 2016.

[67] Tian-Yu Wang, Jia-Lin Meng, Zhen-Yu He, Lin Chen, Hao Zhu, Qing-Qing Sun, Shi-Jin Ding, Peng Zhou, and David Wei Zhang. Fully transparent, flexible and waterproof synapses with pattern recognition in organic environments. *Nanoscale Horizons*, 4(6):1293–1301, 2019.

[68] S. Z. Li, F. Zeng, C. Chen, H. Y. Liu, G. S. Tang, S. Gao, C. Song, Y. S. Lin, F. Pan, and D. Guo. Synaptic plasticity and learning behaviours mimicked through ag interface movement in an ag/conducting polymer/ta memristive system. *Journal of Materials Chemistry C*, 1(34):5292–5298, 2013.

[69] L. Barrio, J. Catalán, and J. L. G. de Paz. Dft study of ionization potentials for aza-substituted aromatic rings. *International Journal of Quantum Chemistry*, 91(3):432–437, 2003.

[70] M. Chattopadhyaya, S. Sen, M. M. Alam, and S. Chakrabarti. The role of relativity and dispersion controlled inter-chain interaction on the band gap of thiophene, selenophene, and tellurophene oligomers. *Journal of Chemical Physics*, 136(9):9, 2012.

[71] Theresa M. McCormick, Colin R. Bridges, Elisa I. Carrera, Paul M. DiCarmine, Gregory L. Gibson, Jon Hollinger, Lisa M. Kozycz, and Dwight S. Seferos. Conjugated polymers: Evaluating dft methods for more accurate orbital energy modeling. *Macromolecules*, 46(10):3879–3886, 2013.

[72] J. Torras, J. Casanovas, and C. Aleman. Reviewing extrapolation procedures of the electronic properties on the pi-conjugated polymer limit. *Journal of Physical Chemistry A*, 116(28):7571–7583, 2012.

[73] Igor Zozoulenko, Amritpal Singh, Sandeep Kumar Singh, Viktor Gueskine, Xavier Crispin, and Magnus Berggren. Polarons, bipolarons, and absorption spectroscopy of pedot. *ACS Applied Polymer Materials*, 1(1):83–94, 2018.

[74] S. Helmy, F. A. Leibfarth, S. Oh, J. E. Poelma, C. J. Hawker, and J. R. de Alaniz. Photoswitching using visible light: A new class of organic photochromic molecules. *Journal of the American Chemical Society*, 136(23):8169–8172, 2014.

[75] G. Koeckelberghs, L. De Cremer, W. Vanormelingen, W. Dehaen, T. Verbiest, A. Persoons, and C. Samyn. Improved synthesis of n-alkyl substituted dithieno 3,2-b : 2 ',3 '-d pyrroles. *Tetrahedron*, 61(3):687–691, 2005.